Steel and Composite Structures, *Vol. 21, No. 2 (2016) 267-287*
DOI: http://dx.doi.org/10.12989/scs.2016.21.2.267

Experimental study on shear capacity of SRC joints with different arrangement and sizes of cross-shaped steel in column

Qiuwei Wang*, Qingxuan Shi and Hehe Tian

College of Civil Engineering, Xi'an University of Architecture and Technology, Xi'an, P.R. China

(*Received October 08, 2015, Revised December 29, 2015, Accepted March 28, 2016*)

Abstract. The seismic performance of the ordinary steel reinforced concrete (SRC) columns has no significant improvement compared to the reinforced concrete (RC) columns mainly because I, H or core cross-shaped steel cannot provide sufficient confinement for core concrete. Two improved SRC columns by constructing with new-type shaped steel were put forward on this background, and they were named as enlarging cross-shaped steel and diagonal cross-shaped steel for short. The seismic behavior and carrying capacity of new-type SRC columns have been researched theoretically and experimentally, while the shear behavior remains unclear when the new-type columns are joined onto SRC beams. This paper presents an experimental study to investigate the shear capacity of new-type SRC joints. For this purpose, four new-type and one ordinary SRC joints under low reversed cyclic loading were tested, and the failure patterns, load-displacement hysteretic curves, joint shear deformation and steel strain were also observed. The ultimate shear force of joint specimens was calculated according to the beam-end counterforce, and effects of steel shape, load angel and structural measures on shear capacity of joints were analyzed. The test results indicate that: (1) the new-type SRC joints display shear failure pattern and has higher shear capacity than the ordinary one; (2) the oblique specimens have good bearing capacity if designed reasonably; and (3) the two proposed construction measures have little effect on the shear capacity of SRC joints embedded with diagonal cross-shaped steel. Based on the mechanism observed from the test, the formulas for calculating ultimate shear capacity considering the main factors (steel web, stirrup and axial compression ratio) were derived, and the calculated results agreed well with the experimental and simulated data.

Keywords: steel reinforced concrete (SRC); beam-column joint; cross-shaped steel; quasi-static test; shear capacity

1. Introduction

Steel reinforced concrete (SRC) structures have gained increasing applications in practical structural engineering because they offer advantages in both structural performance and convenient construction. This system combines the rigidity and formability of reinforced concrete with the strength and construction speed associated with structural steel to produce an economic structure. The concrete used for encasing structure steel not only increases its strength and stiffness but also improves its fire-resistance. The seismic behavior of SRC members and its influence factors have been studied by many researchers at home and abroad (Yasuo *et al*. 2000, Yasushi *et*

*Corresponding author, Associate Professor, Ph.D., E-mail: wqw0815@126.com

 ISSN: 1229-9367 (Print), 1598-6233 (Online)

al. 2004, de Sousa and Caldas 2005, Jiang and Jia 2007, Shim *et al*. 2008, Guo *et al*. 2010, Kim *et al*. 2011, Karimi *et al*. 2012, Zhang *et al*. 2012, Chen *et al*. 2014, Lu *et al*. 2014). The results have shown that SRC columns embedded with I, H or core cross-shaped steel were mainly adopted in the engineering practice while these ordinary shaped steel could provide limited confinement for core concrete, and the seismic performance of the ordinary SRC columns has no significant improvement compared to the reinforced concrete (RC) columns. Two improved SRC columns embedded with new-type shaped steel were developed by authors to overcome the shortcomings of ordinary SRC columns on this background. The first type is a cross-shaped steel whose flanges are in contact with concrete cover (short for "enlarging cross-shaped steel"), and the second type is a rotated cross-shaped steel whose webs coincide with diagonal line of the column's sections (short for "diagonal cross-shaped steel"). Completed experimental studies have shown that the seismic performance of new-type SRC columns is better than that of ordinary ones when other conditions are same (Wang *et al*. 2013).

Beam-column joints in a composite structural system are crucial zones for effective transfer of forces between the connecting elements and significantly affect the seismic performance of structures. Shear failure of the joints is a major reason that leads to structural instability and collapse. During the last two decades, a series of experimental studies were performed by Nishiyama *et al*. (2004), Wang *et al*. (2010), Gan *et al*. (2011), Ma *et al*. (2011) and Fan *et al*. (2014) on composite beam-column joints to investigate their shear behavior. Many types of connection details were examined in their studies, including connections for concrete-filled steel tubular (CFST) column and H-shaped steel beams, connections for SRC column and composite steel-concrete beams, connections for H-shaped steel column and steel beams, connections for reinforced concrete column and composite steel-concrete beams, and connections for H-shaped steel column and steel beams, and it has been observed that composite beam-column joints, reasonably designed, have good resisting shear capacity under earthquake loads.

However, as compared with the above joints, shear behavior of connections for SRC column and SRC beams are seldom studied. In the previous experimental research about SRC beam-column joints, the specimens were primarily designed to have strong joint region and the configurations in core zone, failure modes and ductility on SRC joint were investigated. For example, Chou and Uang (2007) tested two exterior moment connections with SRC column and beams to evaluate the cyclic performance, and the connection forms of steel skeletons were compared. Yan and Jia (2010) investigated the characteristics of six interior SRC frame joint specimens under low cyclically lateral load, and studied the effects of the axial load ratio and volumetric stirrup ratio on the joint performance including failure mode, ductility, energy dissipation capacity and strength degradation. Chen *et al*. (2015) presented an experimental study of six 3D SRC T-shaped column-steel beam hybrid joints under low cyclic reversed loads, by considering different categories of steel configuration types in column cross section and horizontal loading angles, the load-displacement curves, carrying capacity, energy dissipation capacity, ductility and deformation characteristics of the test subassemblies were analyzed. In this situation, the seismic performance of beam-column subassemblage could be explored, while the mechanical behavior of the joint region was not reflected in the experimental results.

Compared with the strong joint specimens, few studies have been done on the SRC weak joint specimens, and the existing research work has been mainly performed on ordinary SRC joints, i.e., the SRC beam and columns embedded with ordinary shaped steel (I, H or core cross-shaped steel). Xue *et al*. (2011) tested seventeen specimens under low cyclic reversed loading to investigate the bearing capacity and failure modes of SRC specially-shaped column-beam joint, formulas for

shear capacity under bend-shear action were put forward through regression analysis of the test data. Jia *et al*. (2013) tested twelve interior steel reinforced high strength concrete (SRHC) beam-column joints under lateral cyclic force and constant axial load, and developed a model to determine the shear strength of interior SRHC beam-column joints considering the main factors.

The advantages of new-type SRC columns have been proved theoretically and experimentally, yet when the new-type columns are jointed onto SRC beams with I-shaped steel, the shear behavior of the beam-column joints remain unclear. For the application of new-type shaped steel in project, this paper presents an experimental study to investigate the shear capacity of SRC joints with different arrangement and sizes of cross-shaped steel in column. The steel skeletons embedded in the beam and column were welded together to transfer the bending moment effectively, and the construction measures were designed according to Chinese specification JGJ 138 (Design code 2001). Tests of four new-type and one ordinary specimens under low reversed cyclic loading were conducted, and test results were evaluated in terms of failure patterns, joint shear deformation, steel strain and ultimate shear force; and based on the mechanism observed from the test, the formulas for calculating ultimate shear capacity considering steel web, stirrup and axial compression ratio were derived.

2. Experimental program

2.1 Test specimens

2.1.1 Specimen design

In order to study the shear capacity of SRC beam-column joints, the design of the joint specimens should obey the principle of "weak joint and strong member" so that the joints display shear failure firstly. This differs from current design codes for structures, and the reason is that the shear capacity should be established based on joint failure. Compared with the strong joint failure mode, the ultimate shear force of the "weak joint" situation is more accurate.

To force the joint damage to occur at the joint region, the beams and columns of the specimens were designed to have approximately equal flexural strength. The test presented in this study consisted of totally five SRC beam-column joints, named as SSRCJ1~SSRCJ5 respectively. The enlarging cross-shaped steel with flanges was adopted for the column of specimen SSRCJ2, and the diagonal one for columns of specimens SSRCJ3~SSRCJ5. The beam was oblique to the column for the specimen SSRCJ3, and the reason was that the oblique layout usually appeared in actual engineering. An ordinary SRC beam-column joint (SSRCJ1) as control specimen was tested for comparison, for which core cross-shaped steel was embedded in the column. The common hot-rolled I-shaped steel was used for beams of SRC joints. The connection forms of steel skeletons are shown in Fig. 1. Dimensions and reinforcement arrangement of all specimens are illustrated in Fig. 2.

In all test specimens, the columns were 2100-mm-high with cross section of 250 mm × 250 mm and the beams were 2750-mm-long with cross section of 200 mm × 300 mm (SSRCJ1) and 220 mm × 300 mm (SSRCJ2~SSRCJ5). The concrete used in the specimens was C50, the embedded steel was type Q235, the reinforcing bars was type HRB400 with 20 mm diameter, and the stirrup was type HPB300 with 6 mm diameter. The concrete cover thickness was 20 mm, and stirrup spacing for the encrypted region, low density zone and joint core area were respectively 30 mm, 50 mm and 100 mm. Different parameters were involved in these specimens to investigate

the influences on the shear behavior of SRC joints, including the steel shape, load angel and construction measures. Table 1 collects the details of the tested specimens.

The steel was cut and machined according to design requirements. In order to ensure the stress transfer of beam-column joints, several holes were opened on the steel web of columns as channels of reinforcing bars in beams because the steel and reinforcing bars intersected for specimens SSRCJ2~SSRCJ5. And meanwhile, the column stirrup in core zone was cut into two parts which were welded on the steel web of beams. Then the reinforcing bars were settled by tying with stirrup to form a reinforced skeleton frame, and formwork support and pouring concrete could be completed on this basis.

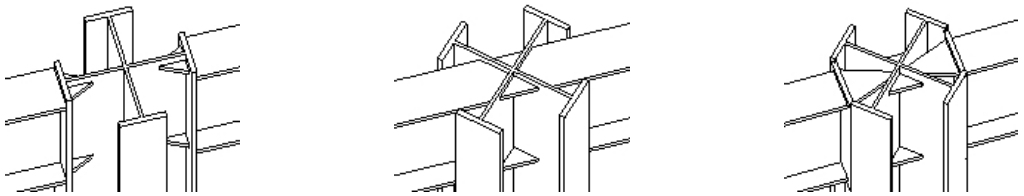

(a)Specimen SSRCJ1~SSRCJ3 (b) Specimen SSRCJ4 (c) Specimen SSRCJ5

Fig. 1 The connection of steel skeletons

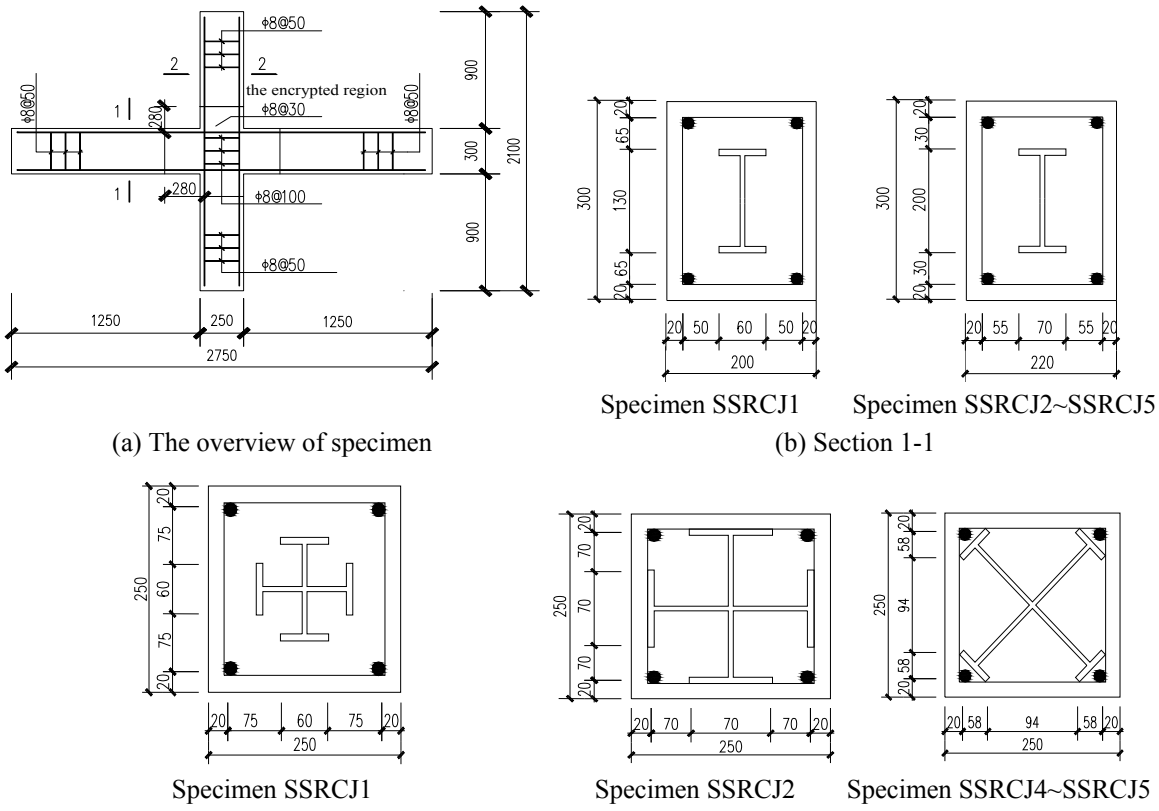

(a) The overview of specimen (b) Section 1-1

(c) Section 2-2

Fig. 2 Geometry and steel arrangement of specimens

Table 1 Specimen sectional dimensions

Specimen	Steel in the column		Steel in the beam		Axial compression ratio n_t^*
	Steel section $h_w \times b_f \times h_f \times t_w^*$(mm^4)	Steel ratio (%)	Steel section $h_w \times b_f \times h_f \times t_w^*$ (mm^4)	Steel ratio (%)	
SSRCJ1	130×60×6×8	6.20	130×60×6×8	3.14	0.40
SSRCJ2	194×70×5×8	7.09	200×70×5×8	3.31	
SSRCJ3	210×70×5×8	7.39	200×70×5×8	3.31	
SSRCJ4	210×70×5×8	7.39	200×70×5×8	3.31	
SSRCJ5	210×70×5×8	7.39	200×70×5×8	3.31	

* $h_w \times b_f \times h_f \times t_w$: b_f and h_f are the flange width and height, and h_w and t_w are the web height and thickness respectively.

* n_t: The experimental axial compression ratio is calculated according to the expression $n_t = N_k/(f_{ck}A_c + f_{ak}A_a)$. Where N_k is the standard value of joint axial compression force; f_{ck} and A_c are the standard values of compressive strength and cross sectional area for concrete; f_{ak} and A_a are respectively the standard values of compressive strength and cross sectional area for steel.

Table 2 Material properties of steel

Material	Grade	Yield strength f_y (MPa)	Ultimate strength f_u (MPa)	Elastic modulus E (MPa)
Steel	Q235	248.3 (t = 5 mm)	388.8	2.0×10^5
		245.5 (t = 6 mm)	395.6	2.0×10^5
		230.6 (t = 8 mm)	388.0	2.0×10^5
Reinforcing bars	HRB400	448.1	613.4	2.0×10^5
Stirrup	HPB300	309.5	480.7	1.7×10^5

Material strength used to evaluate ultimate stress uses the result of the material test. The mechanical properties of steel, reinforcing bars and stirrup from test are listed in Table 2. For the joint specimens, six 150-mm concrete cubic blocks were tested for compressive strength, and the average cubic compressive strength f_{cu} is 51.2 MPa.

2.1.2 Test setup and instrumentation layout

The test setup used for the experimental program is shown in Fig. 3. Columns were pin-connected at their ends to present inflection points at the midspan of the member length. The pinned connection at the bottom of the column was achieved by using a three dimensional spherical plain bearing made specifically for this experiment. The vertical load was applied on the top of column using hydraulic actuators. There were two loading steps in the test, as follows: (1) an axial compression force was firstly induced by a load-jack and maintained constant during the whole course of loading; and (2) a reversed cyclic load was then applied laterally using a MTS hydraulic actuator system. In elastic range, the lateral load was applied with an increment of 20kN, and at each increment one loading cycle was applied to the column. Once yielding was reached, the applied load was a function of the yielding displacement Δ_y, and in this range, three cycles were applied to the column at each displacement increment. The test was stopped until the lateral load reduced to 85% of the ultimate load or the column couldn't keep its stability.

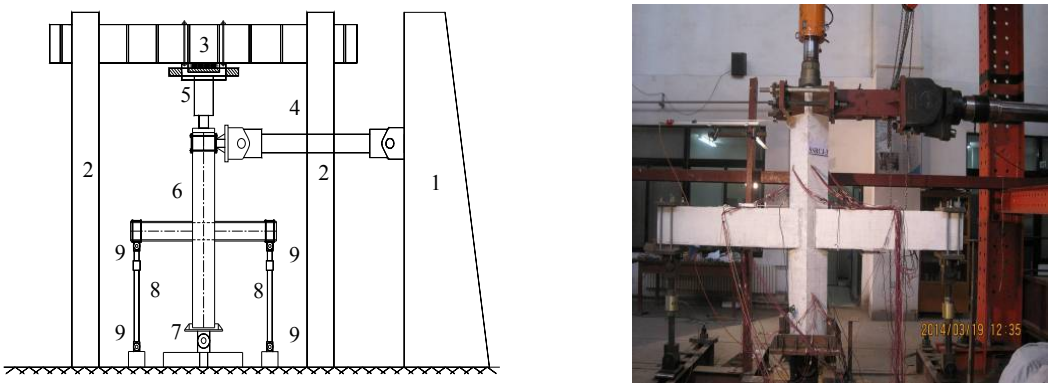

(a) Sketch map (b) Photo of the actual load

1. reaction wall; 2. reaction steel frame; 3. reaction girder; 4. actuator for lateral force; 5. oil jack; 6. test specimen; 7.column hinge device; 8. sensors; 9. beam hinge device

Fig. 3 The test setup

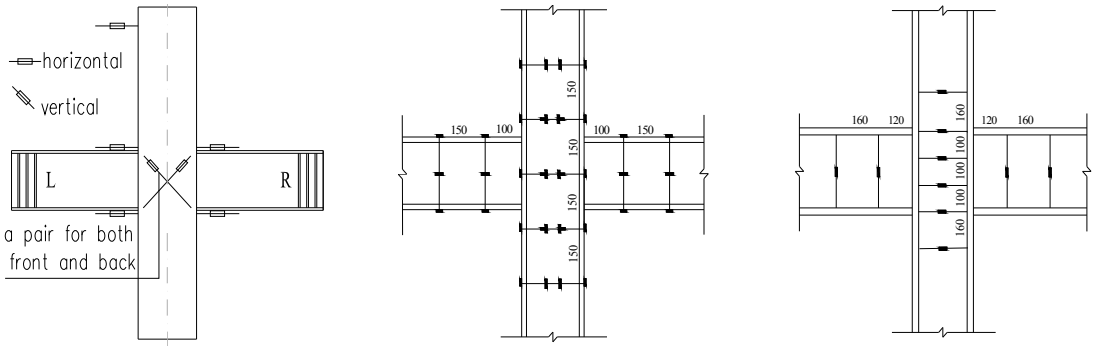

(a) Displacement meters (b) Strain gages for steel and longitudinal reinforcement (c) Strain gages for stirrups

Fig. 4 Measurement points arrangement of specimens

During the test, the lateral load in addition to the displacement and the strain of the steel, reinforcement and stirrup were measured and recorded automatically. The lateral load is measured by the sensor installed on the actuator and the lateral displacement is measured by displacement meters on top of the specimens. The joint shear deformation is measured by two pairs of crossed displacement meters in core area. The main measuring point arrangement is shown in Fig. 4. Meanwhile, displacement meters cannot be set in the joint core region along the diagonal direction for the specimen SSRCJ3, and thus the Fig. 4(a) is only for specimens SSRCJ1~SSRCJ2 and SSRCJ4~SSRCJ5.

2.2 Discussion of test results

2.2.1 Failure patterns

The joint specimens all display shear failure which is consistent with the expected results. Fig. 5 shows the final failure pattern of specimens SSRCJ1~SSRCJ5 under low reversed cyclic loading.

Failure processes of the five specimens are similar and could be divided into elastic, elastic-plastic and plastic stages. The elastic stage is from loading until cracks appearing in the joint core region, and the stirrup and steel web don't yield and the shear force is mainly provided by concrete. The elastic-plastic stage is from the first crack to yielding of the steel web, and the strain of stirrups in the joint increases fast and stirrups of part specimens have yielded during this stage. And finally, the plastic stage is defined as yielding of the steel web to specimen failure, and in this stage, the stirrup has yielded and the specimens are damaged along with concrete crushing.

Apart from the specimen SSRCJ1, the strength decreasing was minor after peak load for other specimens because the concrete area confined by steel in the joint is larger. The failure phenomena were slightly different for new-type SRC joints due to the effect of steel shape, load angle and construction measures. Part of joint core concrete was still complete until the specimen was damaged for specimen SSRCJ2. The beam was oblique to the column for specimen SSRCJ3 whose joint zone includes beam ends and column edges, and diagonal cracks appeared firstly at beam ends in the joint region and then extended to column edges when the specimen was close to yield. The concrete outside of steel flange in the column was so less that the initial crack firstly appeared here, which then extended towards joint core regions for specimens SSRCJ4 and SSRCJ5.

(a) Specimen SSRCJ1

(b) Specimen SSRCJ2

(c) Specimen SSRCJ3

(d) Specimen SSRCJ4

(e) Specimen SSRCJ5

Fig. 5 Failure modes of specimens

Generally, the decline rate of the shear capacity and stiffness for new-type SRC joints (SSRCJ2~SSRCJ5) were slower than those of the ordinary one (SSRCJ1) on every force and displacement level, and the core zone concrete confined by steel could bear larger load and tend to be stable although the specimens were close to failure. This illustrates that the new-type SRC joints have better seismic ductility and resisting shear capacity.

2.2.2 Load-displacement hysteresis curves

The load-displacement curve is an important basis to determine the mechanical behavior. The relationships between the lateral load and displacement for all specimens are shown in Fig. 6, and the following characteristics could be drawn through analysis.

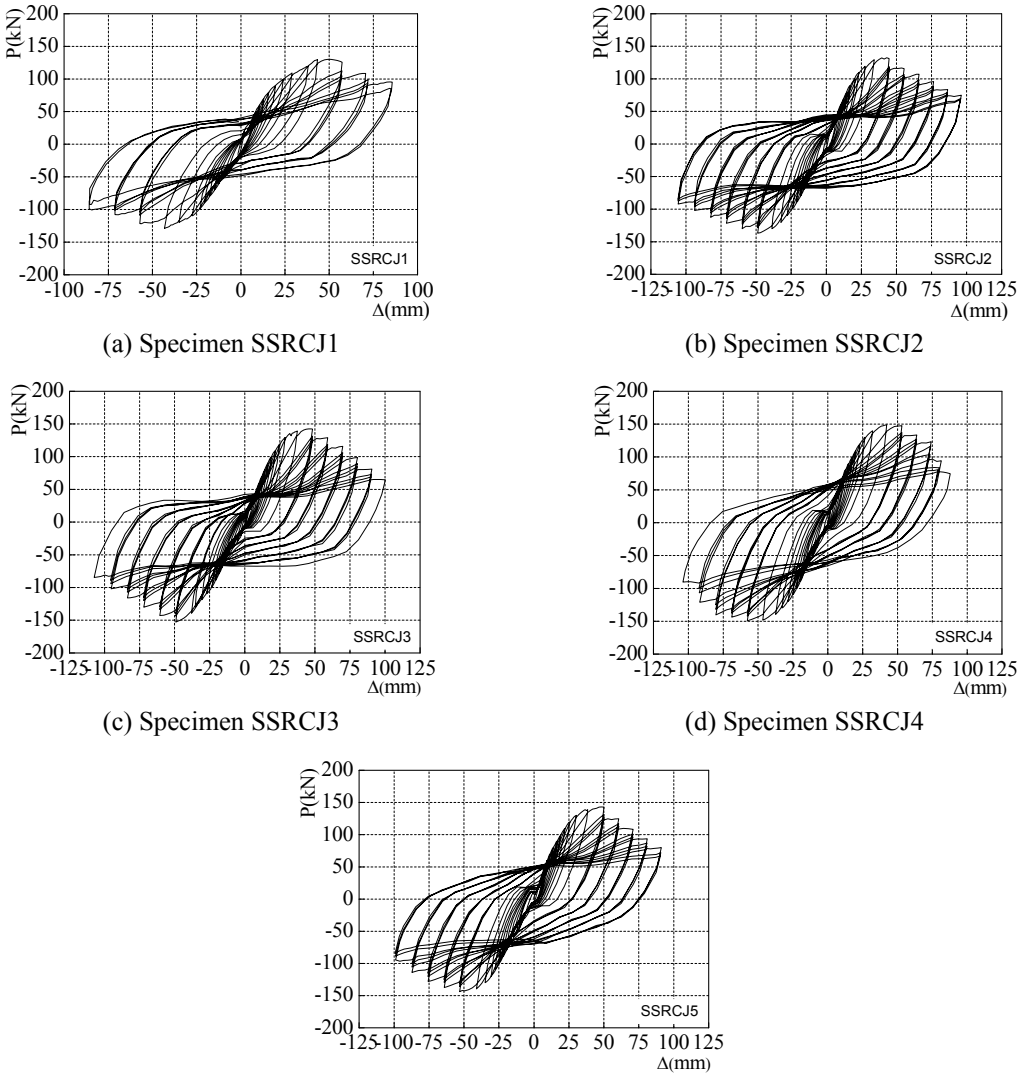

(a) Specimen SSRCJ1

(b) Specimen SSRCJ2

(c) Specimen SSRCJ3

(d) Specimen SSRCJ4

(e) Specimen SSRCJ5

Fig. 6 The hysteretic curves

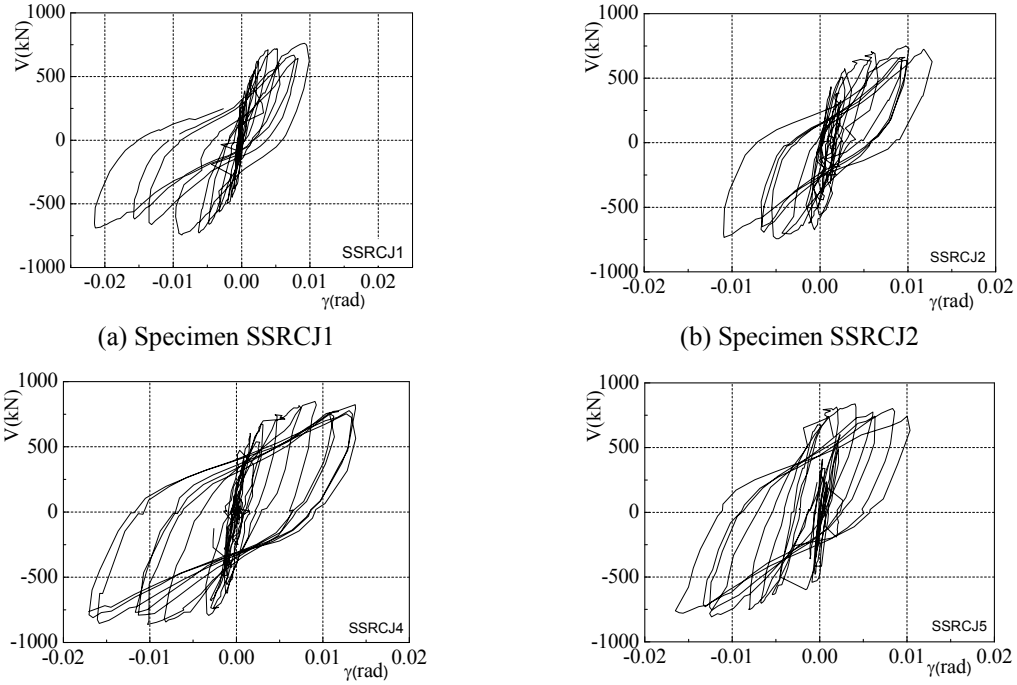

(a) Specimen SSRCJ1 (b) Specimen SSRCJ2

(c) Specimen SSRCJ4 (d) Specimen SSRCJ5

Fig. 7 Shear force (V) versus shear transformation (γ) curves

(1) The specimens behave approximately elastic before the horizontal load increases to the yield load (about 40% of the ultimate load). The stiffness of the specimens decreases slowly from the yield load to the ultimate load and the plastic deformation is small. It is clear that the hysteretic curves start to fall after the ultimate load for all specimens.
(2) The hysteretic loops of the specimens are plump except specimen SSRCJ1 during the elastoplastic range. There is a long level or decline segment after peak value in the envelope curves for specimens SSRCJ2~SSRCJ5, reflecting a strong capacity of plastic deformation and energy dissipation.
(3) The area of hysteretic loop for the specimen SSRCJ1 is smaller than that of specimens SSRCJ2~SSRCJ5 whose strength and stiffness degradation are more serious, illustrating that the energy dissipation of new-type joints is better with high axial compression ratio. The reasons for this phenomenon are mainly summed up into two aspects: one is that enlargement of both area and moment of inertia in new-type section steel is obvious comparing with core cross-shaped steel; and the other is that the enlarging or diagonal cross-shaped steel with flanges could provide larger confinement for concrete in the joint.
(4) The steel shape and construction measures are different for specimens SSRCJ2~SSRCJ5, but there are no significant differences for their hysteretic loops. The reason is that the steel content and confined concrete area in the beam and column are almost equal for the four specimens.

2.2.3 Shear deformation of joints

The shear angle γ is adopted to measure shear deformation of the joint. The relationship

between the shear force (V) and shear angle (γ) can be obtained by theoretical deduction, as shown in Fig. 7. What need to emphasize is that, the ultimate shear angle is denoted by the deformation angle corresponding to 0.92 times peak shear stress, and the reason is that concrete cover spalling is serious at the later loading stage and the ultimate shear angle can't be measured. It can be seen from Fig. 7 that the shear angel increases linearly with the shear force in the initial stage. The curves are becoming nonlinear with the increase of the cyclic number, and more irrecoverable deformation is presented. This shows that the joints are mainly at phase of elastic-plasticity which agrees with the shear failure pattern.

Meanwhile, it can be seen that (1) the negative shear angle of the ordinary SRC joint (SSRCJ1) is slightly larger than that of other specimens with the load increasing, reflecting that the enlarging cross-shaped steel could provide stronger confinement which makes the shear deformation of joints be smaller; and (2) the shear angle of specimens SSRCJ4 and SSRCJ5 is larger compared to other joints, and thus shear deformation of joints embedded with the diagonal cross-shaped steel is more obvious.

2.2.4 Strain of steel web and stirrup

The shear capacity of the specimens is mainly provided by steel web, stirrup and concrete in the joint core. Some strain gauge has been damaged at ultimate capacity state, and limited by the number of effective strain gauge, only several load-strain curves of steel web and stirrup are given, as shown in Fig. 8. It can be seen from Fig. 8 that steel web in the joint core all yielded when the specimens failed. The steel web remained in the elastic condition during the initiation of loading, and the shear force was mainly provided by core zone concrete; the strain of steel web increased fast after cracking, reflecting shear action of the steel web became more evident; with the load increasing, the steel web yielded and was in strain-hardening range gradually, whereafter the shear force of joints was improved, and shear resistant action of the steel was fully explored. By comparison, the steel web of new-type SRC joints yielded earlier whose strain values were greater than that of the ordinary joint, showing that the new-type joints could give full play to the role of steel web.

The strain of stirrups was little changed before cracking, and the stirrup hadn't been subjected to stress in this case. The stirrup strain was small ($< 1\times10^{-3}\varepsilon$) from cracking to yield, and reached the yield point ($1.5\times10^{-3}\varepsilon$) in the ultimate load. With increasing lateral loads and horizontal displacements, it is observed that the concrete began to expand and drop, and the strain

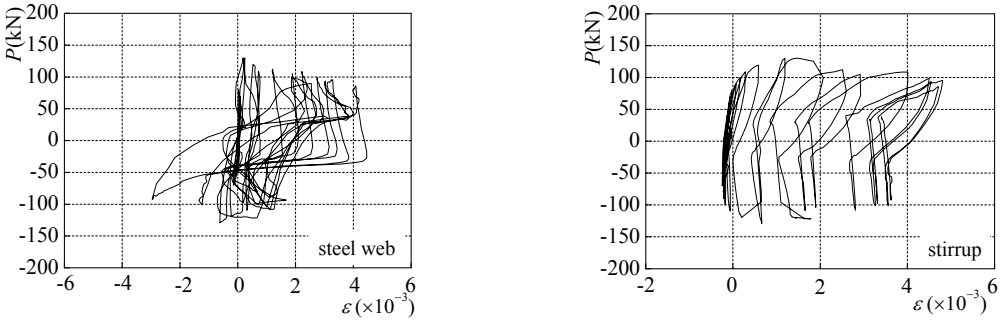

(a) Specimen SSRCJ1

Fig. 8 Load-strain curves of steel web and stirrup in the joint core

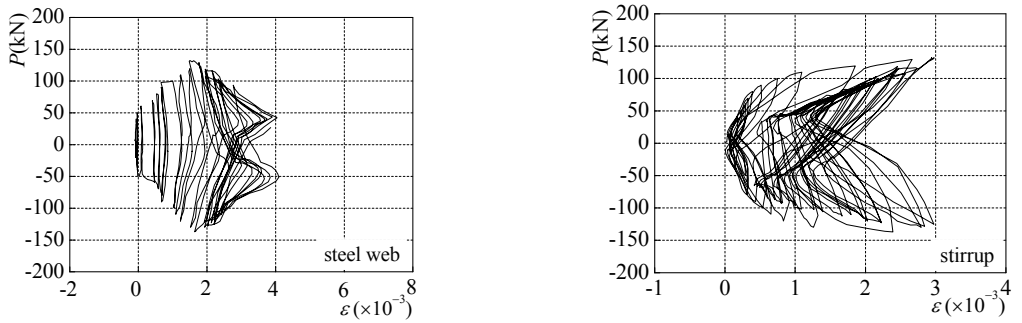

(b) Specimen SSRCJ2

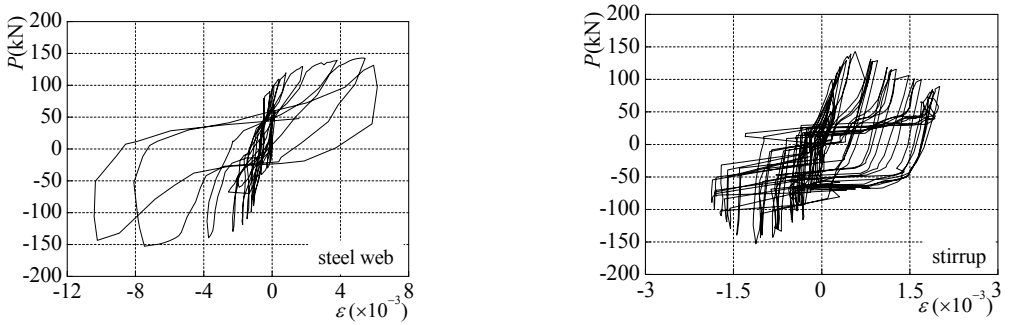

(c) Specimen SSRCJ3

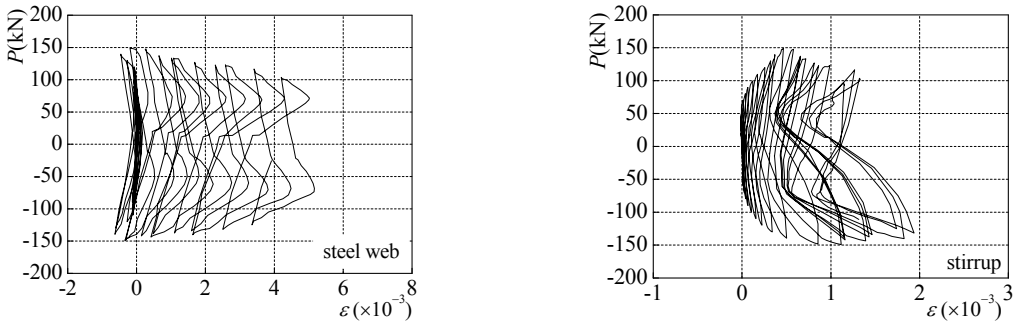

(d) Specimen SSRCJ4

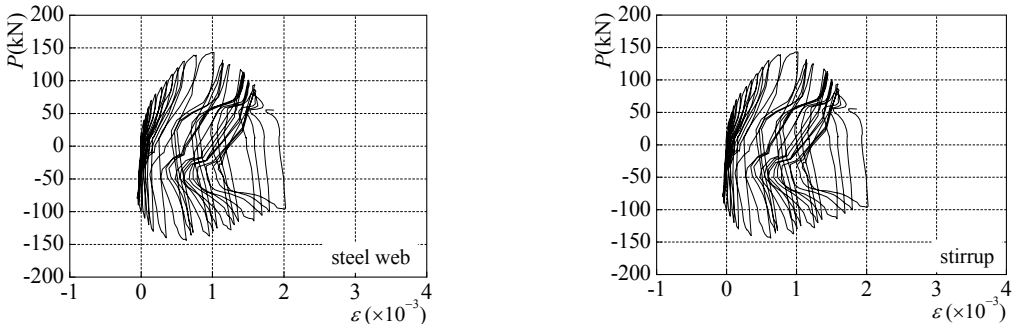

(e) Specimen SSRCJ5

Fig. 8 Continued

of stirrups further increased. This illustrates that stirrups could provide effective confinement to the concrete, thereby to improve the shear capacity of joints.

2.2.5 Ultimate shear force of specimens

A cross section I-I is selected as shown in Fig. 9(a), above which the isolation body will be analyzed. The total horizontal shear of joints can be obtained according to the equilibrium conditions of forces

$$V_{\mathrm{j}} = T_{\mathrm{b}} + C_{\mathrm{b}} - V_{\mathrm{c}} \tag{1}$$

Where T_b and C_b are the tension and pressure from the beam end respectively, and V_c is horizontal shear in the column end. T_b and C_b are determined as

$$T_{\mathrm{b}} = M_{\mathrm{b2}} / h_{\mathrm{bw}}, \quad C_{\mathrm{b}} = M_{\mathrm{b1}} / h_{\mathrm{bw}}$$

Where M_{b1} and M_{b2} are bending moments on the beam end, and h_{bw} is the distance between resultant force points of tension and compression. And therefore V_j is

$$V_{\mathrm{j}} = \frac{M_{\mathrm{b1}} + M_{\mathrm{b2}}}{h_{\mathrm{bw}}} - V_{\mathrm{c}} \tag{2}$$

Where V_c can be calculated by means of the computing unit between inflection points of the upper and lower columns, as shown in Fig. 9(b).

The bending moment at inflection points are zero, and M_{ct} and M_{cb} are as following

$$M_{\mathrm{ct}} = V_{\mathrm{c}} h_1, \quad M_{\mathrm{cb}} = V_{\mathrm{c}} h_2$$

The bending moment at inflection points is zero, and M_{ct} and M_{cb} are as following

$$M_{\mathrm{ct}} + M_{\mathrm{cb}} = M_{\mathrm{b1}} + M_{\mathrm{b2}} \tag{3}$$

And V_c is derived as

$$V_{\mathrm{c}} = \frac{M_{\mathrm{b1}} + M_{\mathrm{b2}}}{h_1 + h_2} = \frac{M_{\mathrm{b1}} + M_{\mathrm{b2}}}{h - h_{\mathrm{b}}} \tag{4}$$

(a) The force model of the joint core (b) The equivalent calculation diagram

Fig. 9 Calculation of the ultimate shear force

Table 3 The ultimate shear force of specimens

Specimen	Counterforce on the beam end		Bending moment on the beam end		The ultimate shear force V_j (kN)
	R_1 (kN)	R_2 (kN)	M_{b1} (kN·m)	M_{b2} (kN·m)	
SSRCJ1	92.99	90.63	111.58	108.76	904.86
SSRCJ2	107.67	83.60	129.20	100.32	942.56
SSRCJ3	116.33	102.00	139.60	122.40	1047.91
SSRCJ4	120.20	98.33	144.24	118.00	1076.90
SSRCJ5	112.33	100.20	134.80	120.24	1075.33

Where M_{ct} and M_{cb} are bending moments of the column ends above and below the node, h_1 and h_2 are the heights of the upper and lower columns between inflection points, h is the distance between inflection points, and h_b is the section height of the beam.

Generating Eq. (4) to Eq. (2), Eq. (5) can be obtained

$$V_{\mathrm{j}} = \frac{M_{\mathrm{b1}} + M_{\mathrm{b2}}}{h_{\mathrm{bw}}}\left(1 - \frac{h_{\mathrm{bw}}}{h - h_{\mathrm{b}}}\right) \tag{5}$$

The beam-end counterforce R_1 and R_2 can be obtained through sensors and data acquisition instruments in the experiment, and bending moments M_{b1} and M_{b2} of the beam end equal the counterforce times corresponding force arms (1.2 m). The ultimate shear force of all joints specimen can be obtained through the Eq. (5). Table 3 shows the calculation results.

It can be seen from Table 3 that (1) the ultimate shear force of new-type SRC joints is much improved than that of the ordinary one (SSRCJ1), and the maximum and minimum extents are respectively 16% (SSRCJ4) and 4% (SSRCJ2); (2) oblique layout makes the concrete area of the joint core be greater, and then the oblique specimen (SSRCJ3) has good resisting shear capacity; and (3) the specimens embedded with diagonal cross-shaped steel (SSRCJ4 and SSRCJ5) have great shear capacity and their values are almost the same, reflecting the two proposed construction measures have little effect on the shear capacity of SRC joints, and this arrangement could enhance the shear resistance ability of steel.

3. Calculation method of shear capacity

3.1 The working mechanism

There is usually two shear mechanism for ordinary SRC beam-column joints: steel-truss mechanism and rigid frame-steel shear wall mechanism. The former involves the shear resistant action of concrete and steel flange while weakens that of the steel web, by contrast, the latter fully considers the shear action of the steel web which divides the SRC joints into two parts, the reinforced concrete and the steel. For the new-type SRC joints, the strut-tie mechanism plays a major role prior to yield, and the shear force that the steel bears is relatively small at the moment. The yield surface of steel web in the joint core is gradually expanding after yield, and the statically indeterminate structure consisted of steel web and flange becomes a geometrical unstable system, which conforms to the "rigid frame-steel shear wall mechanism". As the concrete cracks expanding, the skeletal frame composed of stirrup, steel in the column and the stiffening

provides effective confinement to the concrete, and the combined action of "strut-tie mechanism and restriction mechanism" is formed. In a word, the shear mechanism of new-type SRC joints is the combination of strut-tie mechanism, rigid frame-steel shear wall mechanism and restriction mechanism.

The force mechanism of the SRC beam-column joints is more complex, and according to the experimental results, it is considered that the shear capacity is mainly provided by steel web, stirrup and core concrete. Hence, superimposition method can be used to calculate the shear capacity.

$$V_{\mathrm{j}} = V_{\mathrm{sw}} + V_{\mathrm{sv}} + V_{\mathrm{c}} \tag{6}$$

Where V_j is the shear capacity of SRC joints, V_{sw}, V_{sv} and V_c are the shear force carried by steel web, stirrup and concrete respectively.

3.2 Calculation formulas of shear capacity

3.2.1 Steel web

From the experiments, it can be concluded that the steel web of joint specimens had fully yielded at ultimate capacity state whose shear resistance ability was exploited. The steel web could be regarded as ideal elastic-plastic material which is at the compound condition under the shear and compression loading. The steel web is in elastic state before yield whose principal tensile and compressive stress are as follows

$$\begin{cases} \sigma_1 = \dfrac{\sigma_{\mathrm{cs}}}{2} + \sqrt{(\dfrac{\sigma_{\mathrm{cs}}}{2})^2 + \tau^2} \\ \sigma_3 = \dfrac{\sigma_{\mathrm{cs}}}{2} - \sqrt{(\dfrac{\sigma_{\mathrm{cs}}}{2})^2 + \tau^2} \end{cases} \tag{7}$$

Mises yield condition is suitable for the steel web before the limit state

$$\sqrt{\frac{1}{2}\left[(\sigma_1 - \sigma_2)^2 + (\sigma_2 - \sigma_3)^2 + (\sigma_3 - \sigma_1)^2\right]} \le f_{\mathrm{a}} \tag{8}$$

Where σ_{cs} is the axial compressive stress from columns, f_a is the yield strength of steel. Forces of the steel web are in one plane ($\sigma_2 = 0$), and the shear yield stress of steel web can be obtained by generating Eq. (7) to Eq. (8)

$$\tau = \sqrt{\frac{f_{\mathrm{a}}^2 - \sigma_{\mathrm{cs}}^2}{3}} \tag{9}$$

Thus, shear capacity that the steel web bears is as Eq. (10)

$$V_{s\mathrm{w}} = \tau t_{\mathrm{w}} h_{\mathrm{w}} = \sqrt{\frac{f_{\mathrm{a}}^2 - \sigma_{\mathrm{cs}}^2}{3}} t_{\mathrm{w}} h_{\mathrm{w}} = \xi f_{\mathrm{a}} t_{\mathrm{w}} h_{\mathrm{w}} \tag{10}$$

Where V_{sw} is shear capacity of the steel web, t_w and h_w are respectively thickness and height of the steel web.

The coefficient ξ is introduced into the Eq. (10) which reflects the influences of steel shape and construction measures on shear capacity of the steel web. When the enlarging and diagonal cross-shaped steel are embedded and the oblique layout is adopted, the influence coefficients are denoted by ξ_1, ξ_2 and ξ_3 respectively.

3.2.2 Stirrup

The shear force that the stirrup bears is small when compared to the steel web. Shear resistance ability of the stirrup is mainly presented as: confining concrete in the joint core, limiting the shear deformation and crack development, and delaying the damage processes of the joints. The shear capacity of the stirrup can be calculated according to the method of Chinese specification GB 50010 (Design code 2010), and shear capacity of the stirrup is expressed as Eq. (11)

$$V_{\mathrm{sv}} = \frac{f_{\mathrm{yv}} A_{\mathrm{sv}} (h_0 - a_{\mathrm{s}}')}{s} \tag{11}$$

Where V_{sv} is shear capacity of the stirrup, f_{yv} is the yield strength of stirrup, A_{sv} is the gross area of stirrup in the same section, S is stirrup spacing in the joint core, and $(h_0 - a_s')$ is the distance between the resultant force of tension and compression reinforcement in beams.

3.2.3 Joint core concrete

The joint core concrete forms a compression zone in diagonal direction, and areas among diagonal cracks are becoming concrete strut with load increasing. Shear capacity of the joint core concrete depends on compression strut, whose horizontal component force is the horizontal shear that the joint core concrete bears. The shear capacity of concrete is as Eq. (12)

$$V_{\mathrm{c}} = H b_{\mathrm{j}} f_{\mathrm{c}} \cos\theta \tag{12}$$

Where H is the effective width of concrete compression strut (Fig. 10), θ is the angle between compression strut and horizontal direction, b_j is section width of the joint with a value of $(b_c + b_b)/2$, and b_c and b_b are section width of the column and beam respectively.

H is equal to the diagonal size of the joint times the coefficient α less than 1.0, and it could be expressed as

$$H = \alpha \sqrt{h_{\mathrm{j}}^2 + h_{\mathrm{b}}^2} \tag{13}$$

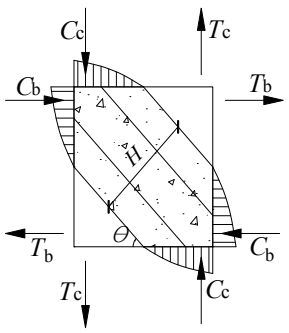

Fig. 10 The concrete compression strut

Where h_j is depth of the horizontal section in the joint (equalling to h_c), h_b is section height of the beam (equalling to h_c times coefficient β, namely $h_b = \beta h_c$). Thus

$$H = \alpha\sqrt{1+\beta^2}\,h_{\mathrm{j}} \tag{14}$$

$$V_{\mathrm{c}} = \alpha\sqrt{1+\beta^2}\,f_{\mathrm{c}}b_{\mathrm{j}}h_{\mathrm{j}}\cos\theta \tag{15}$$

Let be $\gamma = \alpha\sqrt{1+\beta^2}\cos\theta$, and the Eq. (16) could be derived

$$V_{\mathrm{c}} = \gamma f_{\mathrm{c}}b_{\mathrm{j}}h_{\mathrm{j}} \tag{16}$$

Where γ is the influence coefficient of the axial compression ratio on concrete shear capacity. The recent research demonstrates that γ increases with the increasing of axial compression ratio when the concrete strength is constant, while γ alters insignificantly with the change of concrete strength when the axial compression ratio is constant. Thus the coefficient γ could be expressed by the linear relation about axial compression ratio, namely $\gamma = l + kn$. When the enlarging and diagonal cross-shaped steel are embedded and the oblique layout is adopted, the influence coefficients are denoted by γ_1, γ_2 and γ_3 respectively.

Depending on the above analyses, shear capacity of new-type SRC beam-column joints could be obtained by adding up the parts that steel web, stirrup and concrete bears together, as shown in Eq. (17)

$$V_{\mathrm{j}} = \gamma_{\mathrm{i}}f_{\mathrm{c}}b_{\mathrm{j}}h_{\mathrm{j}} + f_{\mathrm{yv}}\frac{A_{\mathrm{sv}}}{s}(h_0 - a'_{\mathrm{s}}) + \xi_{\mathrm{i}}f_{\mathrm{a}}t_{\mathrm{w}}h_{\mathrm{w}}\ (\mathrm{i}=1,2,3) \tag{17}$$

3.3 Determination of correlation coefficients

3.3.1 The influence coefficient ξ

Shear capacity of the three SRC beam-column joints (with enlarging cross-shaped steel, diagonal cross-shaped steel and oblique layout) with different web thickness has been analyzed by method of numerical simulation because the number of specimens is small. The design parameters

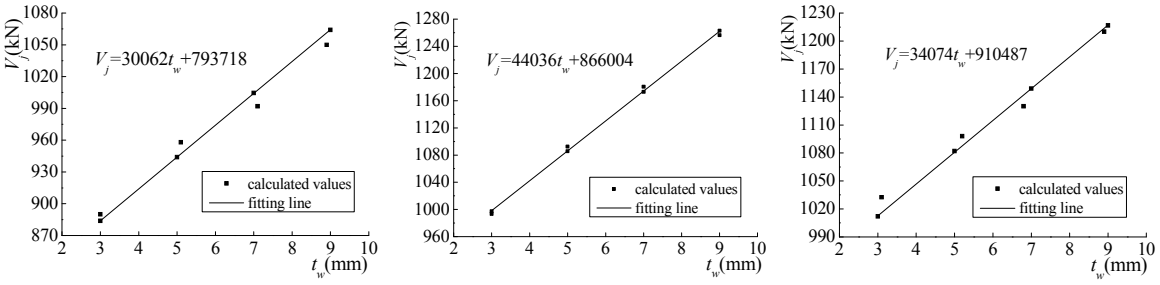

(a) Embedded with enlarging cross-shaped steelh (b) Embedded with diagonal cross-shaped steel (c) The oblique layout

Fig. 11 V_{i}-t_{w} relationship curves

other than steel web are the same with experimental ones. Given space limitations, the process of numerical modeling is omitted here, and more information is in the relevant reference (Tian 2015). The relation between shear capacity V_j and web thickness t_w could be obtained by linearly fitting the calculated data, as shown in Fig. 11. The influence coefficient ξ is equal to expressions in Fig. 11 divided by ($f_a h_w t_w$), and the calculation results are $\xi_1 = 0.66$, $\xi_2 = 0.92$ and $\xi_3 = 0.71$.

3.3.2 The influence coefficient γ

Similarly, shear capacity of three SRC beam-column joints (with enlarging cross-shaped steel, diagonal cross-shaped steel and oblique layout) with different axial compression ratio has been analyzed by the numerical simulation method (Tian 2015). The expression of coefficient γ is

$$\gamma = \frac{V_{\mathrm{j}} - V_{\mathrm{sw}} - V_{\mathrm{sv}}}{f_{\mathrm{c}} b_{\mathrm{j}} h_{\mathrm{j}}} \tag{18}$$

The relation between the influence coefficient γ and axial compression ratio n could be obtained by linearly fitting the calculated data, as shown in Fig. 12. For convenience, the coefficient γ can be approximately described by the following equations

$$\begin{cases} \gamma_1 = 0.34 + 0.04n \\ \gamma_2 = 0.38 + 0.03n \\ \gamma_3 = 0.41 + 0.01n \end{cases} \tag{19}$$

3.4 Verification on the recommended formula

After the influence coefficients ξ and γ are determined, the calculation formula (Eq. (17)) of shear capacity for the three SRC beam-column joints can be specified, and they are as follows.

When the enlarging and diagonal cross-shaped steel are embedded, the shear capacity V_j is as Eqs. (20)-(21)

$$V_{\mathrm{j}} = (0.34 + 0.04n) f_{\mathrm{c}} b_{\mathrm{j}} h_{\mathrm{j}} + f_{\mathrm{yv}} \frac{A_{\mathrm{sv}}}{s} (h_0 - a'_{\mathrm{s}}) + 0.66 f_{\mathrm{a}} t_{\mathrm{w}} h_{\mathrm{w}} \tag{20}$$

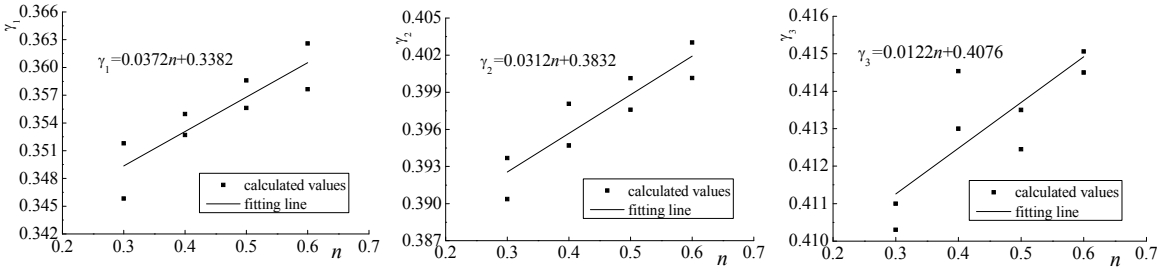

(a) Embedded with enlarging cross-shaped steel

(b) Embedded with diagonal cross-shaped steel

(c) The oblique layout

Fig. 12 γ-n relationship curves

$$V_{\mathrm{j}} = (0.38 + 0.03n) f_{\mathrm{c}} b_{\mathrm{j}} h_{\mathrm{j}} + f_{\mathrm{yv}} \frac{A_{\mathrm{sv}}}{s} (h_0 - a'_{\mathrm{s}}) + 0.92 f_{\mathrm{a}} t_{\mathrm{w}} h_{\mathrm{w}} \tag{21}$$

When the oblique layout is adopted, the shear capacity V_j is as Eq. (22)

$$V_{\mathrm{j}} = (0.41 + 0.01n) f_{\mathrm{c}} b_{\mathrm{j}} h_{\mathrm{j}} + f_{\mathrm{yv}} \frac{A_{\mathrm{sv}}}{s} (h_0 - a'_{\mathrm{s}}) + 0.71 f_{\mathrm{a}} t_{\mathrm{w}} h_{\mathrm{w}} \tag{22}$$

The Eqs. (20)-(22) are available for the joints with 0.2~0.8 axial compression ratio and C30~C80 concrete. Beyond this range, the joint specimens have great brittleness and the calculation equations will not be very suitable. Meanwhile, the anti-seismic adjusting factor of bearing capacity γ_{RE} should be introduced in aseismic design, and the value of γ_{RE} is determined according to the current codes.

The calculated shear capacity of specimens can be obtained by Eqs. (20)-(22). Calculated values have been compared with test results and another group of simulated data, as shown in Tables 4 and 5 respectively. The simulated data is omitted here and more information is in the relevant reference (Tian 2015). It can be seen that the calculated values are corresponding

Table 4 Comparison between calculated results and experimental results for shear capacity

Specimen	Experimental results V_{je} (kN)	Calculated results V_{jc} (kN)	V_{je}/V_{jc}
SSRCJ2	942.56	946.01	1.004
SSRCJ3	1047.91	1080.92	1.032
SSRCJ4	1076.90	1086.71	1.009
SSRCJ5	1075.33	1086.71	1.011

Table 5 Comparison between calculated results and simulated results for shear capacity

Specimen*	Simulated results V_{js} (kN)	Calculated results V_{jc} (kN)	V_{js}/V_{jc}	Specimen	Simulated results V_{js} (kN)	Calculated results V_{jc} (kN)	V_{js}/V_{jc}
SSRCJ2-0.3-5	937.91	936.13	1.002	SSRCJ4-0.3-5	1080.63	1068.18	1.012
SSRCJ2-0.5-5	954.11	949.91	1.004	SSRCJ4-0.5-5	1092.78	1082.70	1.009
SSRCJ2-0.6-5	962.21	957.96	1.004	SSRCJ4-0.6-5	1098.86	1087.85	1.010
SSRCJ2-0.4-3	884.92	882.56	1.003	SSRCJ4-0.4-3	998.50	985.39	1.013
SSRCJ2-0.4-7	1007.10	1003.14	1.004	SSRCJ4-0.4-7	1174.92	1163.43	1.010
SSRCJ2-0.4-9	1068.19	1062.49	1.005	SSRCJ4-0.4-9	1263.13	1246.33	1.013
SSRCJ3-0.3-5	1078.89	1067.42	1.011	SSRCJ5-0.3-5	1080.63	1038.81	1.040
SSRCJ3-0.5-5	1082.94	1071.75	1.010	SSRCJ5-0.5-5	1092.78	1051.35	1.039
SSRCJ3-0.6-5	1084.97	1077.00	1.007	SSRCJ5-0.6-5	1098.86	1056.97	1.040
SSRCJ3-0.4-3	1006.27	1012.84	1.007	SSRCJ5-0.4-3	998.50	956.01	1.044
SSRCJ3-0.4-7	1142.61	1148.99	1.006	SSRCJ5-0.4-7	1174.92	1131.75	1.038
SSRCJ3-0.4-9	1209.93	1217.07	1.006	SSRCJ5-0.4-9	1263.13	1210.67	1.043

well with the experimental and simulated data, and the error is no more than 4%. This illustrates the recommended formulas can accurately predict shear capacity of new-type SRC beam-column joints.

4. Conclusions

Through the experiments on the shear capacity of four new-type and one contrastive SRC joint specimens under low reversed cyclic loading, some conclusions are drawn, as follows:

- The SRC beam-column joint specimens display shear failure mode and the shear deformation at failure is obvious under seismic load. The hysteretic curves of the new-type SRC joints are in plump shapes and have no significant pinch phenomenon, and the degeneration of bearing capacity is slow with the increase of the displacement. Although the specimens are close to failure, the new-type SRC joints could bear larger load and keep better stability than the ordinary one under high vertical load.
- The steel arrangement is an important factor that affects the shear capacity of SRC beam-column joints. Under the same conditions, the ultimate shear force of SRC joints embedded with enlarging and diagonal cross-shaped steel are larger than that embedded with core cross-shaped steel, and the average increasing rate is 4.03% and 16.01% for the two new-type shaped steel. Thus shear behavior of new-type SRC joints has a marked improvement over that of the ordinary one.
- The load angle also affects the shear capacity of SRC joints. The shear capacity of the oblique specimens is poorer than that of the joints embedded with diagonal cross-shaped steel, but better than that of the joints with core and enlarging cross-shaped steel. So it is a fact that the oblique specimens can be used normally if designed properly.
- For the SRC joints embedded with diagonal cross-shaped steel, the two proposed construction measures (adopted in specimens SSRCJ4 and SSRCJ5) have little effect on the shear capacity of specimens. And by contrast, the construction measures adopted by the specimen SSRCJ4 will be easier to be cut and machined from the point of construction.
- The shear mechanism of new-type SRC joints is the combination of strut-tie mechanism, rigid frame-steel shear wall mechanism and restriction mechanism, and steel web, stirrup and axial compression ration are the main factors that affect shear capacity of SRC joints.
- Based on the mechanism observed from the test, the shear force that steel web, stirrup and concrete in the joint core bear is obtained, and the formulas for calculating ultimate shear capacity of the new-type SRC joints are derived by using the regression analysis. The calculated results agree well with the experimental and simulated data, illustrating the recommended formulas is more accurately and can be used in the design and construction of SRC structures.

Acknowledgments

The research described in this paper was supported by Program for Changjiang Scholars and Innovative Research Team in University (PCSIRT13089) and by the National Natural Science Foundation of China (No. 51478382 and No. 51408456). This support is sincerely appreciated.

References

Chen, C.H., Wang, C.K. and Sun, H.Z. (2014), "Experimental study on seismic behavior of full encased steel-concrete composite columns", *J. Struct. Eng.*, **140**(6), 1-10.
Chen, Z.P., Xu, J.J., Chen, Y.L. and Xue, J.Y. (2015), "Seismic behavior of steel reinforced concrete (SRC) T-shaped column-beam planar and 3D hybrid joints under cyclic loads", *Earthq. Struct.*, **8**(3), 555-572.
Chou, C.C. and Uang, C.M. (2007), "Effects of continuity plate and transverse reinforcement on cyclic behavior of SRC moment connections", *J. Struct. Eng.*, **133**(1), 96-104.
de Sousa, B.M.J. Jr. and Caldas, R.B. (2005), "Numerical analysis of composite steel-concrete column of arbitrary cross section", *J. Struct. Eng.*, **131**(11), 1721-1730.
Design code (2001), Technical specification for steel reinforced concrete, JGJ138-2001, Beijing, China.
Design code (2010), Code for design of concrete structures, GB50010-2010, Beijing, China.
Fan, J.S., Li, Q.W., Nie, J.G. and Zhou, H. (2014), "Experimental study on the seismic performance of 3D joints between concrete-filled square steel tubular columns and composite beams", *J. Struct. Eng.*, **140**(12), 1-13.
Gan, D., Guo, L.H., Liu, J.P. and Zhou, X.H. (2011), "Seismic behavior and moment strength of tubed steel reinforced-concrete (SRC) beam-columns", *J. Construct. Steel Res.*, **67**(10), 1516-1524.
Guo, Z.X., Lin, H. and Liu, Y. (2010), "Experimental study on seismic behavior of SRC columns with different stirrup configuration", *J. Build. Struct.*, **31**(4), 110-115. [In Chinese]
Jia, J.Q., Zhu, W.Q. and Wang, J.Z. (2013), "Shear strength of interior steel reinforced high strength concrete beam-column joints", *China Civ. Eng. J.*, **46**(10), 1-8. [In Chinese]
Jiang, R. and Jia, J.Q. (2007), "Seismic ductility of very-high strength-concrete short columns subject to combined axial loading and cyclic lateral loading", *J. Chongqing Univ.* (*English Ed.*), **6**(3), 205-212.
Karimi, K., El-Dakhakhni, W. and Tait, M. (2012), "Behavior of slender steel-concrete composite columns wrapped with FRP jackets", *J. Perform. Construct. Facil.*, **26**(5), 590-599.
Kim, S.H., Jung, C.Y. and Ann, J.H. (2011), "Ultimate strength of composite structure with different degrees of shear connection", *Steel Compos. Struct., Int. J.*, **11**(5), 375-390.
Lu, X.L., Yin, X.W. and Jiang, H.J. (2014), "Experimental study on hysteretic properties of SRC columns with high steel ratio", *Steel Compos. Struct., Int. J.*, **17**(3), 287-303.
Ma, H.W., Jiang, W.S. and Cho, C.D. (2011), "Experimental study on two types of new beam-to-column connections", *Steel Compos. Struct., Int. J.*, **11**(4), 291-305.
Nishiyama, I., Fujimoto, T., Fukumoto, T. and Yoshioka, K. (2004), "Inelastic force-deformation response of joint shear panels in beam-column moment connections to concrete-filled tubes", *J. Struct. Eng.*, **130**(2), 244-252.
Shim, C.S., Chung, Y.S. and Han, J.H. (2008), "Cyclic response of concrete-encased composite columns with low steel ratio", *Proceedings of the Institution of Civil Engineers: Struct. Build.*, **161**(2), 77-89.
Tian, H.H. (2015), "Research on seismic behavior and shear capacity of SRC beam-column joints", Ph.D. Dissertation; Xi'an University of Architecture and Technology, Xi'an, China. [In Chinese]
Wang, T.C., Zhang, X.H., Zhao, H.L. and Qi, J.W. (2010), "Experimental research on seismic behavior of exterior joints with specially shaped columns reinforced by fiber", *Indus. Construct.*, **40**(1), 46-50.
Wang, Q.W., Shi, Q.X., Jiang, W.S., Zhang, X.H., Hou, W. and Tian, Y. (2013), "Experimental study on seismic behavior of steel reinforced concrete columns with new-type cross sections", *J. Build. Struct.*, **34**(8), 18-24. [In Chinese]
Xue, J.Y., Liu Y., Zhao, H.T. and Chen, Z.P. (2011), "Experimental study of the bearing capacity of steel reinforced concrete specially-shaped column-beam joint", *China Civ. Eng. J.*, **44**(5), 41-48. [In Chinese]
Yan, C.W. and Jia, J.Q. (2010), "Seismic performance of steel reinforced ultra high-strength concrete composite frame joints", *Earthq. Eng. Eng. & Vib.*, **9**(3), 439-448.
Yasuo, T., Kaneko, Y. and Yashiro, H. (2000), "Strengthing of reinforced concrete columns by central reinforcing steel element", *Proceedings of 12th World Conference on Earthquake Engineering*, Auckland, New Zealand, January.
Yasushi, N., Shigeyuki, T. and Nozomu, B. (2004), "Flexural behavior of steel reinforced concrete columns

with T-shaped steel", *Proceedings of 13th World Conference on Earthquake Engineering*, Vancouver, BC, Canada, August.
Zhang, S.A., Zhao, Z.Z. and He, X.Q. (2012), "Flexural behavior of SRC columns under axial and bilateral loading", *Appl*. *Mech*. *Mater*., **166**, 3383-3390.

CC